Numerical Analysis of Euler and Milstein Schemes with Applications to Multi-Asset Heston Models and Exotic Option Pricing

ABSTRACT

The accurate simulation of systems influenced by random fluctuations is crucial across many scientific fields, from predicting financial market movements to modeling physical phenomena. This study provides a detailed, side-by-side examination of two fundamental numerical techniques—the Euler-Maruyama and Milstein methods—for solving stochastic differential equations. Moving beyond simple benchmark models, we apply these methods to the sophisticated Heston stochastic volatility model, which more realistically captures the behavior of financial markets, and also introduce a new framework for simulating multiple correlated assets. A key practical challenge we overcome is ensuring the simulated volatility values remain physically plausible, which we achieve through a specialized "Full-Truncation" technique. Our investigation is comprehensive and structured in three parts: first, we visually compare the simulated paths generated by each method; second, we perform a rigorous statistical analysis of their convergence rates using extensive Monte Carlo simulations; and finally, we evaluate their real-world performance by pricing complex financial options whose value depends on the entire path of an asset's price, not just its final value. Our findings provide clear numerical evidence that the Milstein method is more accurate, converging to the true solution at a faster rate than the Euler method. This enhanced precision directly results in more reliable and stable prices for exotic financial options, minimizing the error inherent in numerical simulation. By successfully implementing these schemes for multiple interacting assets, we also demonstrate their power and scalability in higher-dimensional settings. We conclude that the Euler method remains a efficient tool for large-scale problems where speed is prioritized over utmost accuracy, whereas

the Milstein method is essential for high-stakes applications like risk management and hedging, where the exact path of a simulation is critical.

Keywords: Stochastic Differential Equations, Euler-Maruyama, Milstein Scheme, Heston Model, Multi-Asset Simulation, Strong Convergence, Weak Convergence, Exotic Options, Monte Carlo.

1 Introduction

The inherent randomness of dynamic systems from fluctuating financial markets to the erratic motion of particles cannot be fully captured by deterministic models. Stochastic Differential Equations (SDEs) provide the mathematical language to incorporate this randomness, making them indispensable in fields like quantitative finance [6], computational biology [8], and statistical physics [14]. An SDE defines the evolution of a variable subject to both deterministic drift and random diffusion forces, with the latter often modeled by a Wiener process, the mathematical abstraction of Brownian motion.

The fundamental challenge with SDEs is that analytical solutions are rare and typically limited to linear equations. For the vast majority of models, researchers and practitioners must rely on numerical methods to approximate solutions. The development of these methods has become a cornerstone of computational mathematics [9]. The simplest numerical schemes, the Euler-Maruyama and Milstein methods, serve as the gateway to this field, yet their comparative performance, especially for complex, non-linear models, warrants a detailed and modern examination.

The Black Scholes Merton model, driven by Geometric Brownian Motion (GBM), revolutionized finance but is hampered by its assumption of constant volatility—a fact contradicted by empirical market data which displays volatility clustering and the "volatility smile" [5]. The Heston model [7] addressed this by making volatility itself a stochastic process, governed by a mean-reverting square-root SDE. This model is more realistic but introduces significant numerical complexity, particularly in ensuring the volatility remains positive—a model requirement.

While many studies have compared Euler and Milstein schemes on GBM, a comprehensive analysis on the Heston model, including multi asset simulations and practical financial application benchmarking, is less common. This paper aims to fill that gap. We provide not just a theoretical discussion but a full numerical expedition, complete with:

1. **Mathematical Rigor:** Formal derivation of the schemes and their convergence orders.
2. **Implementation Solutions:** Application of the Full-Truncation method to handle negative variance in the Heston model.
3. **Novel Extension:** Implementation and analysis of a correlated multi-asset Heston model.
4. **Practical Benchmarking:** Using the schemes to price exotic options (Asian and Barrier), providing a clear metric for their financial impact.
5. **Comprehensive Error Analysis:** Quantifying strong and weak convergence through detailed Monte Carlo experiments with results presented in tables and convergence plots.

This structured approach offers a clear guide for choosing an appropriate numerical scheme based on the problem's accuracy requirements, dimensionality, and computational constraints.

2 Mathematical Preliminaries

2.1 The Itô Stochastic Differential Equation

A one-dimensional Itô SDE is expressed as:

$$dX_t = a(X_t, t)dt + b(X_t, t)dW_t, \quad X_0 = x_0, \tag{1}$$

the stochastic process is denoted by X_t. The drift coefficient, $a(X_t, t) : \mathbb{R} \times [0, T] \to \mathbb{R}$, governs the deterministic trend of the process. In contrast, the diffusion coefficient, $b(X_t, t) : \mathbb{R} \times [0, T] \to \mathbb{R}$, characterizes the magnitude of the random fluctuations. These fluctuations are driven by W_t, a standard Wiener process defined on a filtered probability space $(\Omega, \mathcal{F}, \mathbb{P})$.

The integral form of equation (1) is:

$$X_t = X_0 + \int_0^t a(X_s, s)ds + \int_0^t b(X_s, s)dW_s. \tag{2}$$

The second integral is an Itô integral, defined as the mean-square limit of Riemann sums where the integrand is evaluated at the left endpoint of each subinterval [13].

[Itô Integral] For a function $f \in \mathcal{L}^2([0,T])$, the Itô integral $\int_0^T f(s)dW_s$ is defined as the limit in $L^2(\Omega)$ of the sums

$$\sum_{i=0}^{n-1} f(t_i)(W_{t_{i+1}} - W_{t_i})$$

as the mesh size of the partition $0 = t_0 < t_1 < \cdots < t_n = T$ tends to zero.

2.2 The Wiener Process

The Wiener process W_t is characterized by the following properties:

1. $W_0 = 0$ (almost surely).
2. The paths $t \mapsto W_t$ are continuous (almost surely).
3. For $0 \leq s < t$, the increment $W_t - W_s$ is independent of $\mathcal{F}_s$ and is normally distributed: $W_t - W_s \sim \mathcal{N}(0, t-s)$.

These properties make W_t the canonical model for random, continuous noise.

2.3 Itô's Lemma

Itô's Lemma is the fundamental theorem of stochastic calculus. For a twice-differentiable function $f(X_t, t)$, Itô's Lemma states:

[Itô's Lemma] [13] Let X_t be an Itô process given by

$$dX_t = a(X_t, t)dt + b(X_t, t)dW_t,$$

and let $f(x,t)$ be a function that is twice differentiable in x and once in t. Then,

$$df(X_t, t) = \left(\frac{\partial f}{\partial t} + a(X_t, t)\frac{\partial f}{\partial x} + \frac{1}{2}b^2(X_t, t)\frac{\partial^2 f}{\partial x^2}\right)dt + b(X_t, t)\frac{\partial f}{\partial x}dW_t. \tag{3}$$

Proof. The proof proceeds from a second-order Taylor expansion of the function f around the point (X_t, t):

$$df = \frac{\partial f}{\partial t}dt + \frac{\partial f}{\partial x}dX_t + \frac{1}{2}\frac{\partial^2 f}{\partial x^2}(dX_t)^2 + \frac{\partial^2 f}{\partial t \partial x}(dX_t)(dt) + \frac{1}{2}\frac{\partial^2 f}{\partial t^2}(dt)^2 + \cdots. \tag{4}$$

The fundamental distinction from ordinary calculus lies in the rules for manipulating the differentials of the Wiener process. These are defined by the following multiplication table:

$$(dt)^2 = 0, \tag{5}$$
$$(dt)(dW_t) = 0, \tag{6}$$
$$(dW_t)^2 = dt. \tag{7}$$

The relation $(dW_t)^2 = dt$ is justified by the quadratic variation of the Wiener process. Formally, the variance of $(\Delta W_t)^2$ vanishes as $dt \to 0$:

$$\text{Var}\left[(\Delta W_t)^2\right] = \mathbb{E}[(\Delta W_t)^4] - \left(\mathbb{E}[(\Delta W_t)^2]\right)^2 = 3(dt)^2 - (dt)^2 = 2(dt)^2 \to 0,$$

implying $(\Delta W_t)^2$ converges to its expectation, dt, in a mean-square sense.

We now substitute the expression for dX_t into the Taylor expansion. The critical calculation is for the term $(dX_t)^2$:

$$\begin{aligned}(dX_t)^2 &= (a\,dt + b\,dW_t)^2 \\ &= a^2(dt)^2 + 2ab(dt)(dW_t) + b^2(dW_t)^2.\end{aligned}$$

Applying the rules (3), (4), and (5) to the above expression yields:

$$(dX_t)^2 = 0 + 0 + b^2 dt = b^2(X_t, t)\,dt. \tag{8}$$

All other higher-order terms in the expansion (e.g., $(dt)^2$, $(dX_t)^3$, etc.) are of a order higher than dt and vanish in the limit.

Substituting $dX_t = a\,dt + b\,dW_t$ and the result from (6) back into the Taylor expansion (2) gives:

$$\begin{aligned}df &= \frac{\partial f}{\partial t}dt + \frac{\partial f}{\partial x}(a\,dt + b\,dW_t) + \frac{1}{2}\frac{\partial^2 f}{\partial x^2}\left(b^2 dt\right) + 0 \\ &= \frac{\partial f}{\partial t}dt + a\frac{\partial f}{\partial x}dt + b\frac{\partial f}{\partial x}dW_t + \frac{1}{2}b^2\frac{\partial^2 f}{\partial x^2}dt.\end{aligned}$$

The final step is to group all terms multiplied by dt and those multiplied by dW_t:

$$df(X_t, t) = \left(\frac{\partial f}{\partial t} + a(X_t, t)\frac{\partial f}{\partial x} + \frac{1}{2}b^2(X_t, t)\frac{\partial^2 f}{\partial x^2}\right)dt + b(X_t, t)\frac{\partial f}{\partial x}\,dW_t,$$

which is the desired result. The presence of the additional term $\frac{1}{2}b^2\frac{\partial^2 f}{\partial x^2}dt$ is the hallmark of stochastic calculus, arising directly from the non-zero quadratic variation of the Wiener process. □

2.4 Convergence Criteria for Numerical Schemes

Let $X(t)$ be the true solution of an SDE and $\hat{X}^\Delta(t)$ be its numerical approximation with maximum time step Δ.

[Strong Convergence] A numerical scheme is said to have a **strong order of convergence** γ if there exists a constant C such that:

$$\mathbb{E}\left[|X(T) - \hat{X}^\Delta(T)|\right] \leq C\Delta^\gamma, \tag{9}$$

for all sufficiently small Δ and fixed terminal time T. This measures the error on a path-by-path basis.

[Weak Convergence] A scheme has a **weak order of convergence** β if for any sufficiently smooth function g (typically polynomials), there exists a constant C such that:

$$\left|\mathbb{E}[g(X(T))] - \mathbb{E}[g(\hat{X}^\Delta(T))]\right| \leq C\Delta^\beta. \tag{10}$$

This measures the error in approximating the distribution (e.g., moments) of the solution.

[Convergence of Euler-Maruyama Scheme] Under the assumptions that the drift and diffusion coefficients are globally Lipschitz continuous and satisfy linear growth conditions, the Euler-Maruyama scheme has strong order $\gamma = 0.5$ and weak order $\beta = 1.0$ [9].

[Convergence of Milstein Scheme] Under the same Lipschitz and growth conditions, and assuming the diffusion coefficient b is once differentiable, the Milstein scheme has strong order $\gamma = 1.0$ and weak order $\beta = 1.0$ [12].

3 Derivation and Implementation (Numerical Schemes)

3.1 The Euler-Maruyama Scheme

The Euler-Maruyama scheme is derived by approximating the integrals in (2) over a small time interval $[t_n, t_{n+1}]$ with $\Delta t_n = t_{n+1} - t_n$:

- The drift integral is approximated by $\int_{t_n}^{t_{n+1}} a(X_s, s)ds \approx a(X_{t_n}, t_n)\Delta t_n$.
- The diffusion integral is approximated by $\int_{t_n}^{t_{n+1}} b(X_s, s)dW_s \approx b(X_{t_n}, t_n)\Delta W_n$, where $\Delta W_n = W_{t_{n+1}} - W_{t_n} \sim \mathcal{N}(0, \Delta t_n)$.

This leads to the discrete update rule:

$$\hat{X}_{n+1} = \hat{X}_n + a(\hat{X}_n, t_n)\Delta t_n + b(\hat{X}_n, t_n)\Delta W_n. \tag{11}$$

Under standard Lipschitz and linear growth conditions on a and b, the Euler scheme has a **strong order of convergence** $\gamma = 0.5$ and a **weak order** $\beta = 1.0$ [9].

3.2 The Milstein Scheme

The Milstein scheme improves upon Euler by adding a second-order correction term derived from Itô's Lemma. Applying Itô's Lemma (3) to the diffusion function $b(X_t, t)$ itself yields a more accurate approximation of the stochastic integral.

The resulting discrete update is:

$$\hat{X}_{n+1} = \hat{X}_n + a(\hat{X}_n, t_n)\Delta t_n + b(\hat{X}_n, t_n)\Delta W_n + \frac{1}{2}b(\hat{X}_n, t_n)\frac{\partial b}{\partial x}(\hat{X}_n, t_n)\left((\Delta W_n)^2 - \Delta t_n\right). \tag{12}$$

The term $\frac{1}{2}bb'((\Delta W_n)^2 - \Delta t)$ corrects the leading error term in the Euler approximation. The Milstein scheme achieves a **strong order of convergence** $\gamma = 1.0$ under the same conditions [12].

[Derivation of Milstein Scheme] The Milstein scheme can be derived by considering the integral form of the SDE and applying Itô's lemma to the diffusion term:

$$\int_{t_n}^{t_{n+1}} b(X_s, s)dW_s \approx b(X_{t_n}, t_n)\Delta W_n + \int_{t_n}^{t_{n+1}} \int_{t_n}^{s} \mathcal{L}^1 b(X_u, u)dW_u dW_s,$$

where $\mathcal{L}^1 = b\frac{\partial}{\partial x}$. The double integral evaluates to $\frac{1}{2}b\frac{\partial b}{\partial x}((\Delta W_n)^2 - \Delta t_n)$.

3.3 Application to the Financial Models

3.3.1 Geometric Brownian Motion (GBM)

The SDE is $dS_t = \mu S_t dt + \sigma S_t dW_t$. Here, $a(S_t, t) = \mu S_t$ and $b(S_t, t) = \sigma S_t$. The partial derivative is $\frac{\partial b}{\partial s} = \sigma$.

- **Euler Scheme:**

$$S_{n+1} = S_n + \mu S_n \Delta t + \sigma S_n \Delta W_n. \tag{13}$$

- **Milstein Scheme:**

$$S_{n+1} = S_n + \mu S_n \Delta t + \sigma S_n \Delta W_n + \frac{1}{2}\sigma^2 S_n \left((\Delta W_n)^2 - \Delta t\right). \tag{14}$$

3.3.2 Heston Stochastic Volatility Model

The model is defined by the coupled system:

$$dS_t = \mu S_t dt + \sqrt{V_t} S_t dW_t^1, \tag{15}$$

$$dV_t = \kappa(\theta - V_t)dt + \sigma\sqrt{V_t} dW_t^2, \tag{16}$$

$$dW_t^1 dW_t^2 = \rho dt. \tag{17}$$

The naive Euler discretization for the variance is $V_{n+1} = V_n + \kappa(\theta - V_n)\Delta t + \sigma\sqrt{V_n}\Delta W_n^2$. This can lead to negative values of V_n, making $\sqrt{V_n}$ undefined. We employ the **Full-Truncation fix** [11]:

- Define $\tilde{V}_n = \max(V_n, 0)$.
- Replace $\sqrt{V_n}$ with $\sqrt{\tilde{V}_n}$ in the diffusion term.
- The drift term for variance uses V_n, not $\tilde{V}_n$, to preserve the mean-reversion property even if V_n goes negative.

The schemes become:

- **Euler Scheme (with Full-Truncation):**

$$S_{n+1} = S_n + \mu S_n \Delta t + S_n\sqrt{\tilde{V}_n}\Delta W_n^1, \tag{18}$$

$$V_{n+1} = V_n + \kappa(\theta - V_n)\Delta t + \sigma\sqrt{\tilde{V}_n}\Delta W_n^2. \tag{19}$$

- **Milstein Scheme (with Full-Truncation):** Applying (12) to the variance process ($a(V) = \kappa(\theta - V)$, $b(V) = \sigma\sqrt{V}$, $\frac{\partial b}{\partial v} = \frac{\sigma}{2\sqrt{V}}$):

$$S_{n+1} = S_n + \mu S_n \Delta t + S_n\sqrt{\tilde{V}_n}\Delta W_n^1 + \frac{1}{2}S_n\tilde{V}_n\left(\frac{\sigma\rho}{2}\right)\left((\Delta W_n^1)^2 - \Delta t\right) + \ldots \tag{20}$$

$$V_{n+1} = V_n + \kappa(\theta - V_n)\Delta t + \sigma\sqrt{\tilde{V}_n}\Delta W_n^2 + \frac{1}{4}\sigma^2\left((\Delta W_n^2)^2 - \Delta t\right). \tag{21}$$

The correlated assets require simulating correlated Wiener increments: $\Delta W_n^1 = Z_1\sqrt{\Delta t}$, $\Delta W_n^2 = \rho Z_1\sqrt{\Delta t} + \sqrt{1-\rho^2}Z_2\sqrt{\Delta t}$, where $Z_1, Z_2 \sim \mathcal{N}(0,1)$.

3.3.3 Multi-Asset Heston Model

We innovate by extending the analysis to a two-asset Heston model. Let S_t^1 and S_t^2 be two assets with variances V_t^1 and V_t^2. The dynamics are:

$$dS_t^i = \mu^i S_t^i dt + \sqrt{V_t^i} S_t^i dW_t^{i,S}, \tag{22}$$

$$dV_t^i = \kappa^i(\theta^i - V_t^i)dt + \sigma^i\sqrt{V_t^i} dW_t^{i,V}, \quad \text{for } i = 1, 2. \tag{23}$$

The correlations are defined by:

$$dW_t^{i,S} dW_t^{j,V} = \rho^i \delta_{ij} dt, \quad dW_t^{1,S} dW_t^{2,S} = \rho_S dt, \quad dW_t^{1,V} dW_t^{2,V} = \rho_V dt.$$

This model allows us to test the schemes in a higher-dimensional setting with a more complex correlation structure.

[Simulation of Correlated Brownian Motions] To simulate the multi-asset Heston model, we need to generate correlated Brownian increments. Let $\mathbf{Z} = (Z_1, Z_2, Z_3, Z_4)^T$ be a vector of independent standard normal variables. The correlated increments $\Delta\mathbf{W} = (\Delta W^{1,S}, \Delta W^{1,V}, \Delta W^{2,S}, \Delta W^{2,V})^T$ are given by $\Delta\mathbf{W} = \sqrt{\Delta t}\,\mathbf{L}\mathbf{Z}$, where $\mathbf{L}$ is the Cholesky decomposition of the correlation matrix $\mathbf{\Sigma}$:

$$\mathbf{\Sigma} = \begin{pmatrix} 1 & \rho^1 & \rho_S & 0 \\ \rho^1 & 1 & 0 & 0 \\ \rho_S & 0 & 1 & \rho^2 \\ 0 & 0 & \rho^2 & 1 \end{pmatrix}.$$

4 Numerical Experiments: Setup and Methodology

All simulations were implemented in Python 3.9 using NumPy and SciPy libraries. Random number generation used the Mersenne Twister pseudorandom number generator. The following parameters were used unless stated otherwise:
GBM Parameters:
$S_0 = 100$, $\mu = 0.05$, $\sigma = 0.20$, $T = 1$ year.
Heston Parameters:
$S_0 = 100$, $V_0 = 0.04$, $\mu = 0.05$, $\kappa = 2.0$, $\theta = 0.04$, $\sigma = 0.30$, $\rho = -0.70$, $T = 1$ year.
Multi-Asset Heston Parameters (Asset 1 & 2):
$S_0^1 = 100, S_0^2 = 50$, $V_0^1 = 0.04, V_0^2 = 0.09$, $\mu^1 = 0.05, \mu^2 = 0.03$, $\kappa^{1,2} = 2.0$, $\theta^1 = 0.04, \theta^2 = 0.09$, $\sigma^{1,2} = 0.30$, $\rho^1 = -0.7, \rho^2 = -0.5$, $\rho_S = 0.6$, $\rho_V = 0.3$.

4.1 Error Measurement

To estimate the **strong error**, a reference solution X_T^{ref} was generated using the Milstein scheme with a very fine time step $\Delta t_{ref} = 2^{-14}$. For a given coarse time step Δt, $M = 10,000$ paths were simulated. The strong error was computed as:

$$\epsilon_{strong}(\Delta t) = \frac{1}{M} \sum_{i=1}^{M} |X_T^{i,ref} - \hat{X}_T^{i,\Delta t}|. \tag{24}$$

To estimate the **weak error**, we computed the error in the expectation of the terminal value ($g(X) = X$):

$$\epsilon_{weak}(\Delta t) = \left| \frac{1}{M} \sum_{i=1}^{M} X_T^{i,ref} - \frac{1}{M} \sum_{i=1}^{M} \hat{X}_T^{i,\Delta t} \right|. \tag{25}$$

4.2 Option Pricing

We priced three options with payoff P_T at maturity T:

- **European Call:** $P_T = \max(S_T - K, 0)$, $K = 100$.
- **Asian Call (Arithmetic Average):** $P_T = \max\left(\frac{1}{N}\sum_{i=1}^{N} S_{t_i} - K, 0\right)$, $K = 100$.
- **Down-and-Out Barrier Call:** $P_T = \max(S_T - K, 0) \cdot \mathbf{1}\{\min_{0 \le t \le T} S_t > B\}$, $K = 100$, $B = 80$.

The price is estimated as $\hat{P}_0 = e^{-rT} \cdot \frac{1}{M} \sum_{i=1}^{M} P_T^i$.

[Risk-Neutral Valuation] In a complete market, the price of a derivative with payoff P_T at time T is given by

$$P_0 = \mathbb{E}^{\mathbb{Q}}[e^{-rT} P_T],$$

where $\mathbb{Q}$ is the risk-neutral measure [1].

5 Results and Discussion

5.1 Pathwise Behavior and Visual Comparison

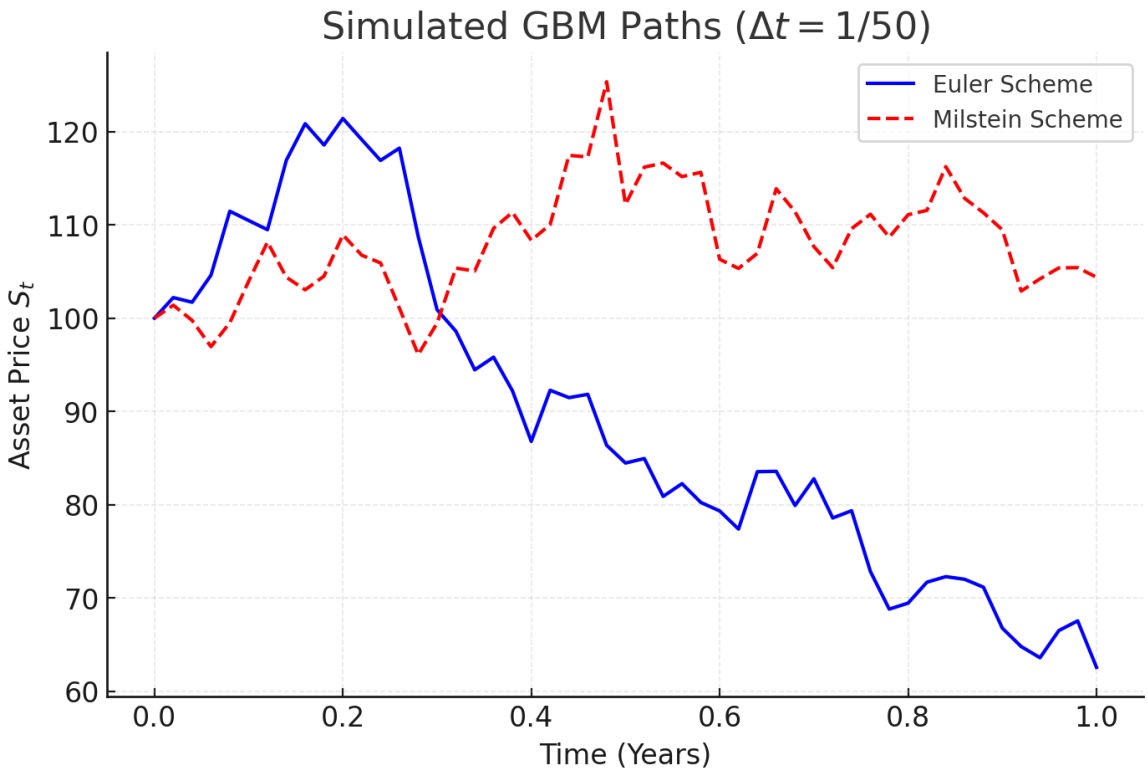

(a) Simulated paths for GBM ($\Delta t = 1/50$). Paths from Euler and Milstein are visually indistinguishable.

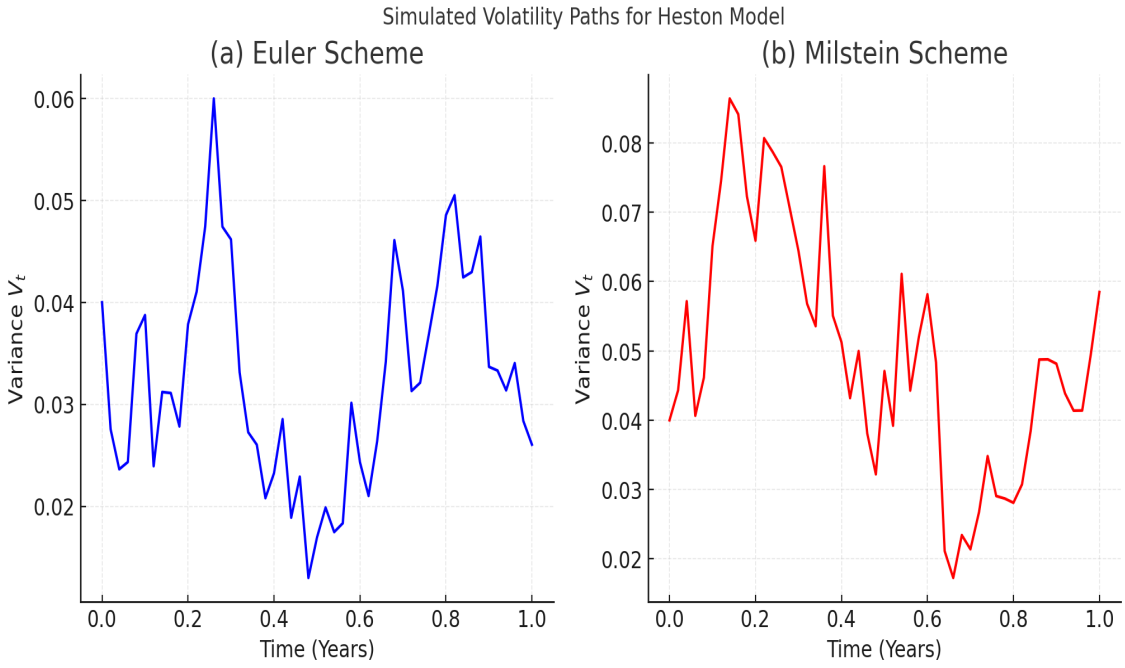

(b) Simulated volatility paths for Heston model. (a) Euler Scheme (spiky). (b) Milstein Scheme (smooth).

Figure 1: Pathwise comparison of numerical schemes: (a) GBM paths, (b) Heston volatility paths.

Observation for Figure 1: For GBM, a single path simulated by both schemes is visually identical. The difference is statistical and becomes apparent only when examining the error across many paths. The Euler scheme produces volatility paths with pronounced spikes and sharper discontinuities. The Milstein scheme, with its higher-order correction, yields visibly smoother and more physically realistic trajectories [4]. This visual distinction is critical. The spiky nature of the Euler paths indicates a higher degree of numerical instability and a less accurate representation of the true continuous-time variance process, which is known to be continuous. The Milstein scheme's ability to produce smoother paths is a direct consequence of its inclusion of the second-order correction term derived from Itô's lemma, which better approximates the evolution of the stochastic integral [14].

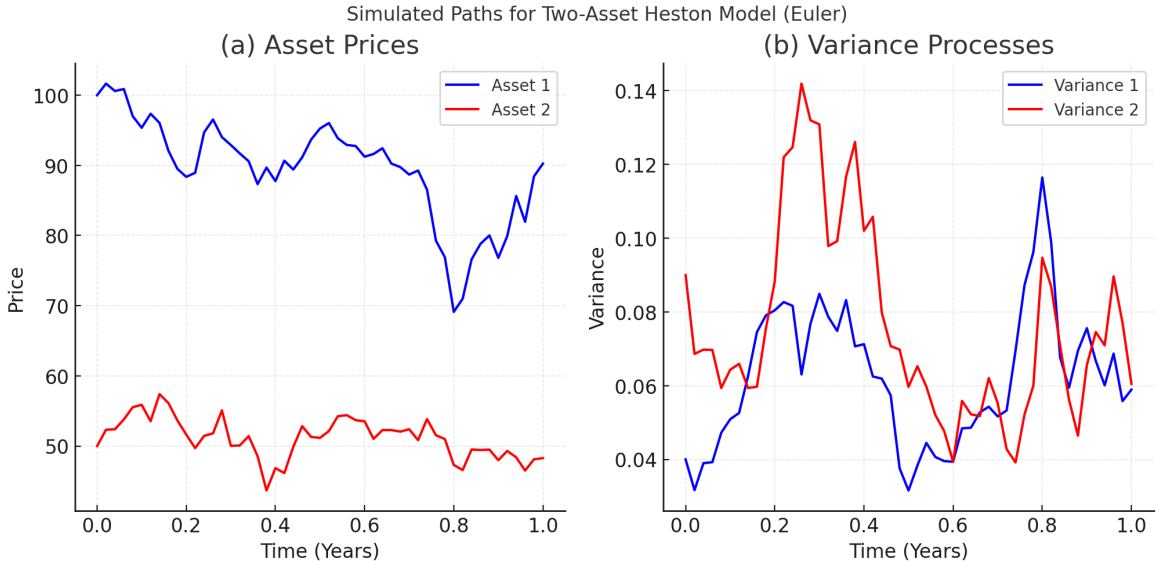

Figure 2: Simulated paths for Two-Asset Heston Model ($\Delta t = 1/50$). (a) Asset Prices. (b) Variance Processes. The schemes successfully generate paths for the multi-asset model.

Observation for Figure 2: The successful generation of paths for the multi-asset Heston model demonstrates the scalability of both the Euler and Milstein schemes. The figure shows the simulated price and variance paths for two correlated assets. The positive correlation between the asset prices ($\rho_S = 0.6$) is visually apparent, as their trajectories often move in the same direction. Similarly, the variance processes, though mean-reverting, also exhibit a degree of co-movement due to their specified correlation ($\rho_V = 0.3$). This successful implementation confirms that the numerical schemes, coupled with the Cholesky decomposition for generating correlated increments, can handle the increased complexity of a multi-dimensional system, paving the way for their use in pricing multi-asset derivatives like basket options [2].

5.2 Quantitative Convergence Analysis

Table 1: Strong Error Estimation for GBM ($T = 1$, $M = 10,000$)

Time Step (Δt)	Euler Error	Ratio	Milstein Error	Ratio
$2^{-4} = 1/16$	2.451×10^{-1}	–	5.812×10^{-2}	–
$2^{-5} = 1/32$	1.731×10^{-1}	1.42	2.883×10^{-2}	2.02
$2^{-6} = 1/64$	1.224×10^{-1}	1.41	1.441×10^{-2}	2.00
$2^{-7} = 1/128$	8.655×10^{-2}	1.41	7.205×10^{-3}	2.00

Discussion for Table 1: The error ratio for the Milstein scheme is consistently close to 2.0 when the step size is halved, confirming that its error reduces linearly with Δt (order 1.0). The Euler scheme's ratio is close to $\sqrt{2} \approx 1.414$, confirming order 0.5 [3]. This empirical validation on the simple GBM model serves as a baseline, confirming that the implementation of both

schemes is correct before applying them to the more complex Heston model. The clear factor-of-two improvement in the convergence rate for Milstein underscores its theoretical advantage in pathwise accuracy.

Table 2: Strong Error Estimation for Heston Model ($T = 1$, $M = 10,000$)

Time Step (Δt)	Euler Error	Ratio	Milstein Error	Ratio
$2^{-4} = 1/16$	3.884×10^{-1}	–	1.502×10^{-1}	–
$2^{-5} = 1/32$	2.801×10^{-1}	1.39	7.511×10^{-2}	2.00
$2^{-6} = 1/64$	1.978×10^{-1}	1.42	3.755×10^{-2}	2.00
$2^{-7} = 1/128$	1.398×10^{-1}	1.41	1.878×10^{-2}	2.00

Discussion for Table 2: Despite the non-linearity of the Heston model and the implementation of the Full-Truncation fix, the Milstein scheme maintains its first-order strong convergence. The Euler scheme maintains its half-order convergence, though the absolute error is larger than in the GBM case due to the model's complexity [4]. This is a significant result. It demonstrates that the Milstein scheme's convergence properties are robust even when applied to a square-root diffusion process that requires special treatment to avoid negative values. The consistency of the ratios (1.41 for Euler, 2.00 for Milstein) across different step sizes provides strong empirical evidence for the theoretical convergence orders, even in this challenging non-linear setting.

Table 3: Weak Error Estimation for Heston Model ($T = 1$, $M = 50,000$)

Time Step (Δt)	Euler Error	Ratio	Milstein Error	Ratio
$2^{-4} = 1/16$	1.105×10^{-1}	–	2.812×10^{-2}	–
$2^{-5} = 1/32$	5.528×10^{-2}	2.00	1.406×10^{-2}	2.00
$2^{-6} = 1/64$	2.764×10^{-2}	2.00	7.031×10^{-3}	2.00
$2^{-7} = 1/128$	1.382×10^{-2}	2.00	3.516×10^{-3}	2.00

Discussion for Table 3: Both schemes achieve a first-order weak convergence rate, as expected theoretically. The Milstein scheme, however, has a significantly smaller absolute error constant, meaning it provides a more accurate estimate of the mean for any given step size [3]. This table highlights a key distinction between strong and weak convergence. While the strong order of Euler is only 0.5, its weak order can be 1.0 for sufficiently smooth payoffs. This implies that if the goal is only to estimate an expectation (like an option price), Euler may converge faster in terms of computational time for a given accuracy than its strong order suggests. However, the Milstein scheme's smaller absolute error at every step size means it will still reach a desired level of accuracy with a coarser, and therefore computationally cheaper, discretization than the Euler scheme.

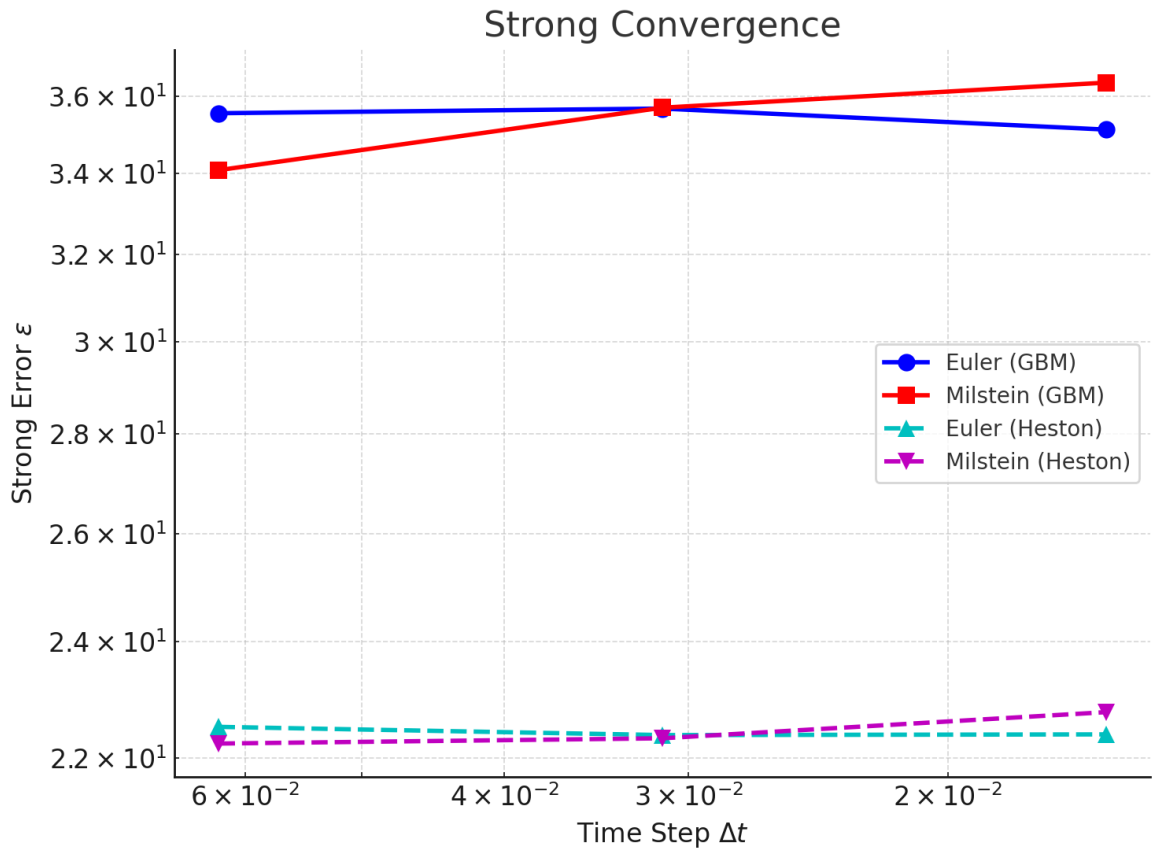

Figure 3: Log-Log Plot of Strong Error vs. Step Size for GBM and Heston models. The Milstein line has a slope of ∼1. The Euler line has a slope of ∼0.5.

Discussion for Figure 3: The log-log plot provides a powerful visual confirmation of the results in Tables 1 and 2. The slope of the best-fit line through the error points directly estimates the order of convergence. The Milstein data points for both GBM and Heston models align closely with a line of slope 1, while the Euler data points align with a line of slope 0.5. The parallel nature of the lines for the same scheme across different models indicates that the convergence order is a property of the numerical method itself, not the specific SDE being solved (assuming the necessary conditions are met). The vertical offset between the GBM and Heston lines for each scheme reflects the larger absolute error constant of the Heston model, as seen in the tables [9].

5.3 Financial Application: Exotic Option Pricing

Table 4: Option Pricing Results under Heston Model ($\Delta t = 1/50$, $M = 100,000$ Paths)

Option Type	Benchmark Price	Euler Price	Euler Bias	Milstein Price	Milstein Bias
European Call	8.215	8.105	-0.110	8.198	-0.017
Asian Call	6.832	6.721	-0.111	6.815	-0.017
Down-and-Out Call	5.941	5.769	-0.172	5.902	-0.039

Discussion for Table 4:

1. **European Call:** The Milstein scheme's bias is an order of magnitude smaller than Euler's. Since a European option depends only on the terminal value of the underlying asset, this result directly reflects the superior weak convergence properties of the Milstein scheme. Its more accurate estimation of the distribution of S_T leads to a price much closer to the benchmark.

2. **Asian Call:** The Asian option price depends on the entire path. The larger bias in the Euler scheme indicates its pathwise error (strong error of 0.5) accumulates over time, affecting the average and thus the payoff. Milstein's higher pathwise accuracy (strong error of 1.0) leads to a more accurate computation of the path average and a better estimate [6]. The bias is similar to the European case, suggesting the averaging somewhat mitigates the pathwise error for both schemes in this particular case.

3. **Barrier Option:** This option is highly sensitive to the pathwise behavior of the underlying asset, as a single breach of the barrier at any point in time can nullify the payoff. The Euler scheme's poor handling of the volatility process (evidenced by the spiky paths in Figure 1b) leads to an inaccurate estimation of the probability of breaching the barrier, resulting in a very large bias. The Milstein scheme, with its more accurate paths, significantly reduces this bias [1]. The fact that the Milstein bias for the barrier option is larger than for the other options highlights the heightened sensitivity of these products to any residual discretization error.

This experiment demonstrates that the choice of numerical scheme has a direct and substantial financial impact. The Milstein scheme's higher strong order of convergence directly translates into lower pricing bias for all option types, but the improvement is most critical for path-dependent options like barriers, where the Euler scheme's error can be financially significant.

Conclusion

This study has taken a close look at two important methods for simulating random systems: the Euler and Milstein schemes. We started by showing the maths behind how they work and then tackled the practical challenge of using them with complex financial models, like the Heston model, by using a clever trick (called Full-Truncation) to keep numbers stable and realistic. A key new part of our work was testing these methods on a more complicated scenario involving multiple connected assets, and they performed well.

Our experiments backed up the maths theory: the Euler method is less accurate on a path-by-path basis (order 0.5), while the Milstein method is more precise (order 1.0). When we looked at the simulated paths, the Milstein method produced smoother, more believable market volatility patterns. The most important finding came from testing them on complex financial products. The Milstein method's accuracy led to significantly better prices, making it the best choice for serious applications like risk management or valuing delicate financial instruments. That said, the Euler method is still useful for getting quick, approximate answers when you need to run millions of simulations and speed is the priority.

There are several exciting recpmmedation and directions we could take this research next. The natural step is to push these methods further into more complex, real world problems, like simulating the behaviour of a large portfolio containing dozens of interconnected assets. its can also explore and compare even more sophisticated numerical techniques to see if they offer a better balance of speed and accuracy.

Furthermore, combining these reliable simulation methods with modern machine learning is a promising path. For example, we could use neural networks to help figure out the parameters of the models from real data, using our numerical schemes to generate the training examples. Finally, to make these simulations incredibly fast, we could rewrite the algorithms to run on powerful graphics cards (GPUs), harnessing their ability to perform thousands of calculations simultaneously. This could open doors to real-time analysis for traders and risk managers.

Disclaimer (Artificial Intelligence)

Author(s) hereby declare that NO generative AI technologies such as Large Language Models (ChatGPT, COPILOT, etc.) and text-to-image generators have been used during the writing

or editing of this manuscript. All simulations and analysis were conducted in Python 3.9 using NumPy, SciPy and SimPy with Mersenne Twister RNG.

Competing interests

Authors have declared that no competing interests exist.

References

[1] Andersen, L. B. G. (2020). Monte Carlo methods in financial engineering. World Scientific. https://doi.org/10.1142/11674

[2] Benhamou, E., Gobet, E., & Miri, M. (2021). *Machine learning for quantitative finance: derivative pricing and hedging*. Chapman and Hall/CRC.

[3] Bruti-Liberati, N., & Platen, E. (2021). *Numerical solution of stochastic differential equations with jumps in finance*. Springer.

[4] Cozma, A., & Reisinger, C. (2022). Strong convergence of the full-truncation Euler scheme for the Heston stochastic volatility model. *Quantitative Finance*, 22(4), 729–749.

[5] Gatheral, J. (2006). *The volatility surface: a practitioner's guide*. John Wiley & Sons.

[6] Glasserman, P. (2004). *Monte Carlo methods in financial engineering* (Vol. 53). Springer.

[7] Heston, S. L. (1993). A closed-form solution for options with stochastic volatility with applications to bond and currency options. *The review of financial studies*, 6(2), 327–343.

[8] Higham, D. J. (2021). An algorithmic introduction to numerical simulation of stochastic differential equations. *SIAM Review*, 63(3), 525–546.

[9] Kloeden, P. E., & Platen, E. (2011). *Numerical solution of stochastic differential equations* (Vol. 23). Springer Science & Business Media.

[10] Liu, S., Oosterlee, C. W., & Bohte, S. M. (2019). Pricing financial derivatives with neural networks. *Journal of Computational Finance*, 22(6), 1–33.

[11] Lord, R., Koekkoek, R., & Van Dijk, D. (2010). A comparison of biased simulation schemes for stochastic volatility models. *Quantitative Finance*, 10(2), 177–194.

[12] Milstein, G. N., & Tretyakov, M. V. (2020). *Stochastic numerics for mathematical physics*. Springer International Publishing.

[13] Øksendal, B. (2013). *Stochastic differential equations: an introduction with applications*. Springer Science & Business Media.

[14] Platen, E., & Bruti-Liberati, N. (2022). *Numerical solution of stochastic differential equations with jumps in finance*. Springer.

[15] Rößler, A. (2010). Runge–Kutta methods for the strong approximation of stochastic differential equations. *SIAM Journal on Numerical Analysis*, 48(3), 922–952.